International Journal of Physics and Mathematical Sciences ISSN: 2277-2111 (Online)
An Online, International Journal, Available at http://www.cibtech.org/jpms.htm
2023 Vol. 13, pp. 1-5/Amit et al.
Research Article (Open Access)

STRUCTURAL AND ELASTIC PROPERTIES OF NANOCRYSTALLINE SPINEL FERRITES PREPARED BY HIGH ENERGY BALL MILLING METHOD

***Amit N Maheta[1], K P Thummer[2], Kunal B. Modi[1], Hiren H. Joshi[1]**
[1]Department of Physics, Saurashtra University, Rajkot 360 005, India
[2]Department of Electronics, Saurashtra University, Rajkot 360 005, India
**Author for Correspondence: amitmaheta11@gmail.com*

ABSTRACT
To investigate the influence of Aluminium and Chromium substitution in Magnesium ferrite the spinel system $MgAl_xCr_xFe_{2-2x}$ O_4, (x = 0.1, 0.5 and 0.7) is prepared by standard double sintering ceramic method and further to reduce crystallite size high energy ball mill technique is deployed for 6 Hrs. The structural properties of these milled samples are investigated by X-ray diffraction then to obtain cation distribution Rietveld refinement of XRD data is used. The elastic properties were measured by using Fourier Transform Infrared spectroscopy. The XRD data reveal pure and single-phase ferrites. The value of the lattice constant is increasing as aluminium and chromium content increases.

Keywords: *Magnesium ferrite, Al/Cr substitution, High-energy ball milling, Rietveld refinement, Cation distribution, Structural and Elastic properties*

INTRODUCTION
The properties of the nano-scale materials change drastically as compared to their bulk counterparts (Caizer, and Aliofkhazraei, 2015; Smit, & Wijn, 1954). They can be synthesized by different techniques viz. high energy ball milling, hydrothermal method, sol-gel method, co-precipitation method and citrate-gel method. In recent years ions substituted, nano ferrites catch the attention of researchers across the globe due to their excellent properties which can be controlled by preparation techniques, surface morphology, types and concentration of cation and their distribution at tetrahedral and octahedral sites and excellent chemical stability (Devi & Maisnam, 2020; Houbi, *et al.*, 2021; Niu, *et al.*, 2023). Because of these extraordinary properties, they are broadly used in ferrofluids, radio devices, information storage, chemical technology, fuel cells and some pharmaceutical processes (Bid, S. *et al.*, 2003; Mostafa, M. *et al.*, 2022). Among many ferrites Magnesium ferrite ($MgFe_2O_4$) is a most unique ferrite, due to its high resistivity and low eddy current. It has a cubic structure which crystallizes into a normal spinel structure. (Vishwarup, *et al.*, 2020). To investigate the influence of Aluminium and Chromium substitution in Magnesium ferrite the spinel system $MgAl_xCr_xFe_{2-2x}$ O_4, (x = 0.1, 0.5 and 0.7) is prepared by standard double sintering ceramic method and further to reduce crystallite size high energy ball mill technique, which is relatively simple and inexpensive is deployed for 6 Hrs (Mirbagheri, *et al.*, 2023)

MATERIALS AND METHODS
$MgAl_xCr_xFe_{2-2x}$ O_4, (x = 0.1, 0.5 and 0.7) ferrites were synthesised by low-cost, environment-friendly standard double sintering ceramic method (Thummer, *et al.*, 2004), followed by high energy ball milling which is a famous top-down method to synthesize nano particles. (Mostafa, *et al.*, 2022). In the ceramic method, the oxides of metal ions like MgO, Al_2O_3, Cr_2O_3 and Fe_2O_3 supplied by E. Merck were taken into stoichiometric proportion and mixtures of these powders were done in an agate mortar and pestle for 2 h by using acetone as a blending medium. The mixture was dried at 350K and pressed into compact pellets by applying 2.5-ton pressure. These pellets were kept at 1273.15 K temperature in the furnace for 18 hrs for the pre-sintering process and then cooled slowly to room temperature at the rate of 400K/hour in the final sintering process, the pellets, after re-grinding and repelletizing, were kept at 1473.15K in a furnace for 24 hrs and taken to room temperature by the same cooling rate. This sample was then mechanically milled with acetone as a blending medium for 6 hrs using a Fritsch- Germany-

made high-energy planetary ball mill (Pulverisette 6). The powder: ball ratio of 1:8 was selected and the rotational speed is set at 300 rotations per minute. Finally, the synthesized particles were dried in a furnace at 350K. The structural properties of these milled samples are investigated by X-ray diffraction then to obtain cation distribution Rietveld refinement of XRD data is used. The elastic properties were measured by using Fourier Transform Infrared spectroscopy using FT-IR spectrometer with Potassium bromide (KBr) at room temperature.

RESULTS AND DISCUSSIONS

X-ray diffraction and structural parameters

The structural characterization of the nanocrystal ferrites was carried out by using the PANalytical X'PERT-PRO X-ray diffractometer with Copper K(alpha) radiation. The average crystallite sizes reported were determined by XRD measurements and Scherrer's equation (Thakur, A. *et al.*, 2007). The diffraction angle range was 10° –90° (2θ) with a step of 0.01° at a scan speed of 2°/min. The powder XRD patterns of samples showed the characteristic peaks for the spinel structure. The most intensive diffraction peaks that correspond to the characteristic crystallographic planes of the simple spinel structure of ferrites are (1 1 1),(2 2 0), (3 1 1), (4 0 0), (4 2 2), (3 3 3),(4 4 0), and (5 3 3). The lattice parameter is ranging from8.3750Å to 8.3870Å and it increases with increasing x but this system is not obeying Vegard's law (Thakur, *et al.,* 2020). It is interesting to note that the peak corresponding to (111) reflection appears for $x \geq 0.5$ compositions as well as its intensity also increases with substitution (x) in the system but it is not affected by the milling process. This intriguing phenomenon can be explained based on the atomic scattering factor and site occupancy of various cations distributed among the tetrahedral (*A*-) and octahedral (*B*-) sites of the spinel lattice.

It is found that "Chi-squared" or χ^2 for different compositions lies in the range 1.29 -1.49. The χ^2 values obtained in the present analysis suggest good refinement of the data. The Rietveld agreement factors for x = 0.1, 0.5 and 0.7 are summarized in Table 1.0.

Table 1: Rietveld agreement factors for $MgAl_xCr_xFe_{2-2x}O_4$ system.

Lattice constant, Rietveld reliability factors and Goodness of fit (GOF)				
Content (X)	**lattice constant(Å)**	**R_{wp}(%)**	**R_{exp}(%)**	**GOF**
0.1	8.378	4.90	3.78	1.29
0.5	8.384	5.59	4.12	1.35
0.7	8.400	8.03	5.38	1.49

From the Rietveld analysis, it is confirmed that Chromium occupies Octahedral sites while Aluminium occupies maximum in Tetrahedral sites, which shows less effect of milling on the prepared spinel system (Chhaya, U. V. *et al.,* 1999), and Cation distribution obtained from Rietveld analysis is given in Table 2.0.

Table 2: Cation Distribution from Rietveld method for $MgAl_xCr_xFe_{2-2x}O_4$ system.

Content (*x*)	Composition Formula	A-site	B-site
0.1	$MgAl_{0.1}Cr_{0.1}Fe_{1.8}O_4$	$Mg_{0.14}Al_{0.1}Fe_{0.8}$	$Mg_{0.86}Cr_{0.1}Fe_{1.0}$
0.5	$MgAl_{0.5}Cr_{0.5}Fe_1O_4$	$Mg_{0.14}Al_{0.35}Fe_{0.52}$	$Mg_{0.86}Al_{0.15}Cr_{0.5}Fe_{0.48}$
0.7	$MgAl_{0.7}Cr_{0.7}Fe_{0.6}O_4$	$Mg_{0.14}Al_{0.5}Fe_{0.4}$	$Mg_{0.86}Al_{0.2}Cr_{0.7}Fe_{0.2}$

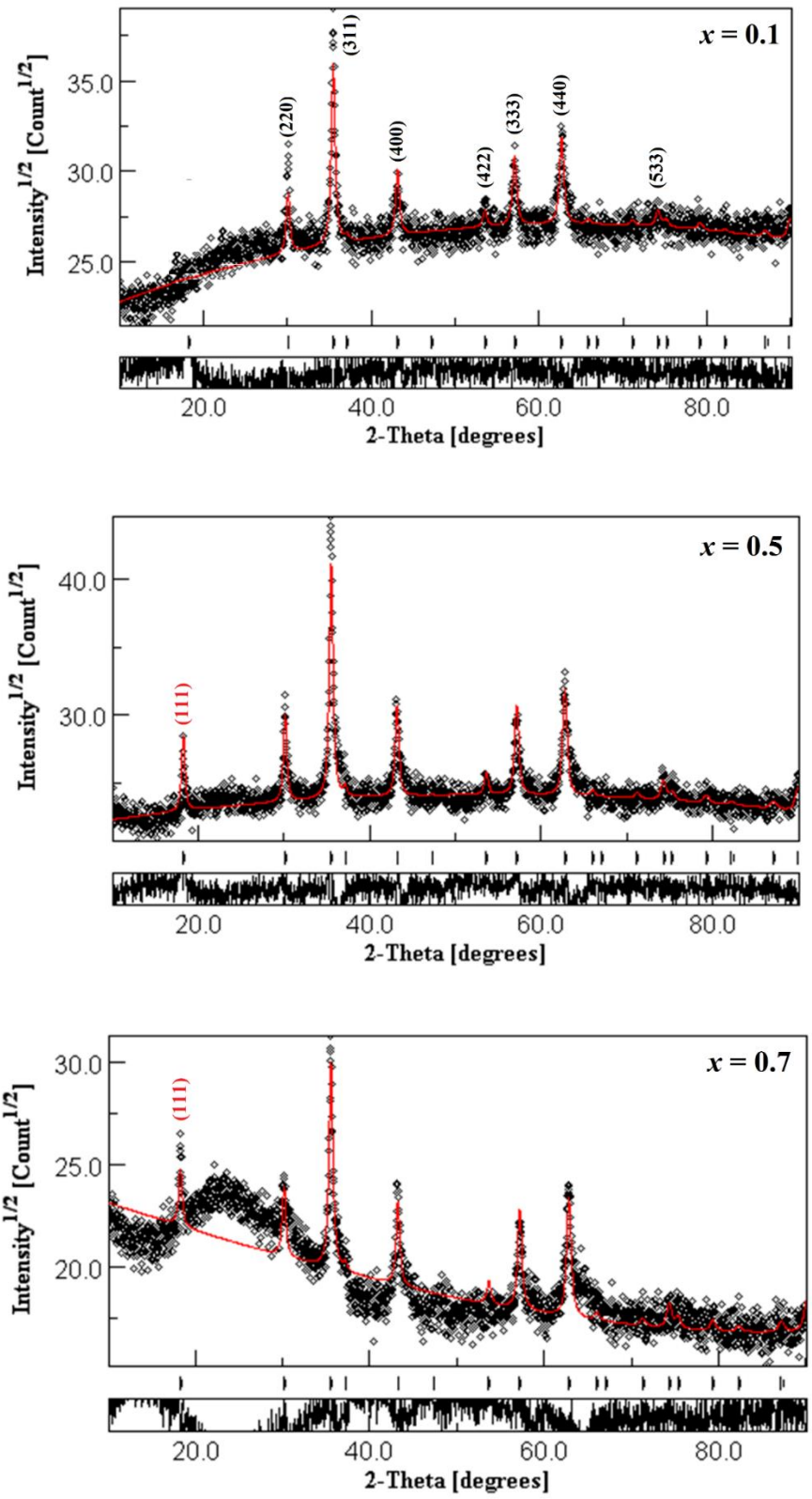

Figure 1: Rietveld-fitted XRD patterns for x = 0.1, 0.5 and 0.7 compositions

Further cation distribution of each sample is used to calculate the value of the mean ionic radius per molecule of the tetrahedral and octahedral sites and also lattice constant obtained theoretically

(Thummer *et al.*, 2017) is well matched with calculated values, which supports cation distribution derived from Rietveld analysis.
It is seen that both radii decrease as aluminium and chromium content are added. We found controversy that lattice constant increases and ionic radii decrease and the major reason behind this is the thermal expansion due to high temperature. Theoretically calculated lattice constant by using the following equation are give in Table 3.0.
$a_{th}=8/3\sqrt{3}[(r_A+R_0)+\sqrt{3}(r_B+R_0)]$
where Ro is the radius of oxygen ion (1.32 Å**)**
Theoretically calculated lattice constant follows the same trend as practically obtained but values are found to be very small due to the reason that theory follows perfect closed pack structure listed in Table 3.0

Table 3: Crystallitesize, Lattice constant(a_{th}) and Mean ionic radii from Cation Distribution for $MgAl_xCr_xFe_{2-2x}O_4$ system.

Lattice constant and Ionic radii					
Content(X)	**Crystallite size(nm)**	**a_{th} (Å)**	**r_A (Å)**	**r_B (Å)**	**r_{avg} (Å)**
0.1	23.25	8.128	0.6554	0.6353	0.6453
0.5	34.73	8.132	0.6037	0.6204	0.6195
0.7	23.65	8.250	0.6034	0.6193	0.6113

Using the XRD data X-ray density (ρ_x), Bulk density (ρ) of the samples were calculated and the percentage of porosity of the samples was calculated by using X-ray density (ρ_x), Bulk density (ρ).
The X-ray density (ρ_x) decreases with aluminium and chromium substitution which is due to small ionic radii of aluminium(Al^{3+}) and chromium (Cr^{3+}) compared to Fe^{+3}ions. Bulk density (ρ) are smaller than that of X-ray density (ρ_x) which is mainly due to pores present in the prepared samples. These are listed in Table 4.0

Table 4: X-ray density (ρ_x), Bulk density (ρ) and Porosity for $MgAl_xCr_xFe_{2-2x}O_4$ system.

X-ray density (ρ_x), Bulk density (ρ) and Porosity			
Content (X)	**(ρx) (g/cm^3)**	**(ρ) (g/cm^3)**	**Porosity**
0.1	4.42	3.09	30.48
0.5	4.14	2.78	33.17
0.7	4.00	2.76	31.22

Infrared Spectroscopy
Ferrites with mineral spinel structure ($MgAl_2O_4$) crystallize in the cubic form with space group Fd^3m-Oh^7 (Bhatu, *et al.*, 2007). The Fourier Transform Infrared Spectroscopy (FTIR) analysis is used at room temperature and the FTIR spectra of the samples are recorded in the wave number range 400 cm^{-1} to 2000 $cm^{-1}$are displayed in Fig.2.0
It is well known that two fundamental absorption bands are seen in the FTIR spectrum of spinel ferrites (O'horo, *et al.*, 1973). The broad band observed at a higher frequency ~ 590 cm^{-1} is attributed to the stretching vibration of (A) site metal-oxygen (M-O) bonds. The band due to the stretching vibration mode of [B] site M-O bonds appears at ~ 405cm^{-1} (Modi, *et al.*, 2006). This indicates that the sample is a cubic spinel ferrite.
The force constants for the tetrahedral site and octahedral site are calculated by using the method suggested by Waldron (Waldron, 1955).

$k_t = 7.62 \times M_1 \times \nu_1^2 \times 10^{-7}$ N/m
$k_o = 10.62 \times M_2/2 \times \nu_2^2 \times 10^{-7}$ N/m
where M_1 and M_2 are the molecular weights of cations on the A-sites and B-sites respectively.

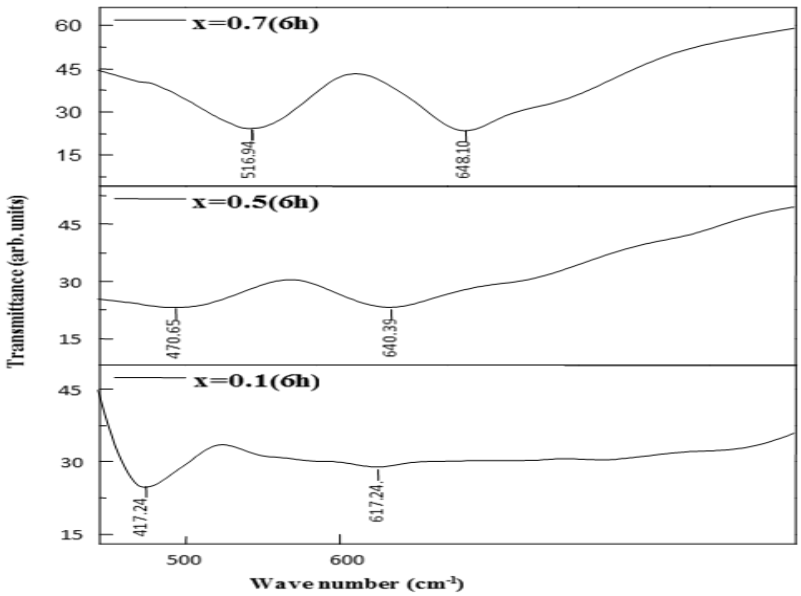

Figure 2: FTIR spectra of $MgAl_xCr_xFe_{2-2x}O_4$ system for x = 0.1, 0.5 and 0.7 compositions

For a better understanding of the mechanical properties of prepared solid ferrites, the elastic constants which are very important in engineering practice like Bulk modulus which describes the ability of a material to resist any change in its volume., modulus of rigidity or shear modulus which shows the ability of a material to resist any change in its shape while maintaining its volume and Poisson's ratio which is the ratio of transverse strain to the longitudinal strain is calculated by using absorption bands obtained in FTIR spectra (Kakani and Hemrajani, 2017) and given in Table 4.0

Table 4: Absorption bands, Force constants, Bulk modulus(B), Modulus of Rigidity(G), and Poisson's ratio(σ)

Content	Absorption bands(cm^{-1})		Force constants(N/m)*10^2			B	G	σ
(x)	ν_1	ν_2	k_t	k_o	k_{avg}		(GPa)	
0.1	617.24	417.24	4.77	3.54	4.15	49.59	17.76	0.220
0.5	640.39	470.65	4.08	3.45	3.77	44.09	16.41	0.211
0.7	648.10	516.94	3.87	3.79	3.83	45.59	16.42	0.218

It is found from the calculation that Poisson's ratio remains invariant (0.21) for all different compositions and is within the standard theoretical range (-1 to 0.5).
The interatomic distances between the cation (b, c, d, e and f) and between the cation and anion (p, q, r and s) were calculated using the following equations

M_e-O
$p = a(1/2-u)$
$q = a(u-1/8)3^{1/2}$
$r = a(u-1/8)11^{1/2}$
$s = a/3(u+1/2)3^{1/2}$

M_e-M_p
$b = (a/4)2^{1/2}$
$c = (a/8)11^{1/2}$
$d = (a/4)3^{1/2}$
$e = (3a/8)3^{1/2}$
$f = (a/4)6^{1/2}$

The bond angles (θ_1, θ_2, θ_3, θ_4 and θ_5) were calculated by following equations

$\theta_1 = \cos^{-1}(p^2+q^2-c^2/2pq)$
$\theta_2 = \cos^{-1}(p^2+r^2-e^2/2pr)$
$\theta_3 = \cos^{-1}(2p^2-b^2/2p^2)$
$\theta_4 = \cos^{-1}(p^2+s^2-f^2/2ps)$
$\theta_5 = \cos^{-1}(r^2+q^2-d^2/2qr)$

Table 5: Interatomic distances and bond angles for $MgAl_xCr_xFe_{2-2x}O_4$ system.

Interatomic Distances (Å) and Bond angles (degrees)			
x	**0.1**	**0.5**	**0.7**
b	2.96207	2.964192	2.969848
c	3.47333	3.475823	3.482456
d	3.62778	3.630378	3.637307
e	5.44167	5.44557	5.45596
f	5.130456	5.134131	5.143928
p	1.981974	1.997758	2.001259
q	2.008792	1.985349	1.989677
r	3.846543	3.801653	3.809942
s	3.692748	3.687098	3.694315
θ1	120.995	121.533	121.522
θ2	135.566	137.565	137.521
θ3	96.705	95.803	95.783
θ4	126.744	126.551	126.556
θ5	111.525	110.2028	110.237

From Table 5 it is observed that the interatomic distances between the cation (b, c, d, e and f) increase while the distance between the cation and anion (p, q, r and s) decreases with doping concentration and the bond angles θ1 and θ2 increases which suggest weakening the interactions while θ3,θ4 and θ5 decreases with aluminium and chromium content added suggests strengthening interactions.

CONCLUSIONS

The paper presents the structural and elastic properties of a high-energy ball-milled spinel ferrite $MgAl_xCr_xFe_{2-2x}$ O_4 system. Rietveld analysis revealed cation distribution and shows chromium occupies only octahedral sites while aluminium occupies both tetrahedral and octahedral sites. The χ^2 values obtained in the range of 1.29 -1.49 shows a good refinement of the data. The value of the lattice constant is found to increase as aluminium and chromium content increases. Theoretically calculated lattice constant shows the same trend as practically obtained. FTIR shows the absorption bands within the standard range of spinel ferrites which confirm that prepared samples have cubic spinel structures.

REFERENCES

Caizer, C., and M. Aliofkhazraei (2015). Handbook of nanoparticles. "*Springer, Switzerland* **201**(5) 481.

Smit, J., & Wijn, H. P. J. (1954). Physical properties of ferrites. In *Advances in Electronics and Electron Physics*, Academic Press. **6, 69-136**.

Devi, N. P., & Maisnam, M. (2020). Characterizations of sol-gel synthesized and high energy ball milled spinel nano ferrites: MFe2O4 (M= Li, Ni, Zn, Mn) for nanofluid preparations. *Integrated Ferroelectrics*, **204**(1), 133-141.

Houbi, A., Aldashevich, Z. A., Atassi, Y., Telmanovna, Z. B., Saule, M., & Kubanych, K. (2021). Microwave absorbing properties of ferrites and their composites: A review. *Journal of Magnetism and Magnetic Materials*, **529**, 167839.

Niu, X., Liu, C., & Zong, B. (2023). Investigation on the microstructure and magnetic properties of Mg (Ga2− x Fe x) O4 spinel ferrites. *Journal of Materials Science: Materials in Electronics*, **34**(2), 118.

Bid, S., & Pradhan, S. K. **(2003).** Preparation of zinc ferrite by high-energy ball-milling and microstructure characterization by Rietveld's analysis. *Materials Chemistry and Physics*, **82**(1), 27-37.

Mostafa, M., Saleh, O., Henaish, A. M., Abd El-Kareem, S. A., Ghazy, R., Hemeda, O. M., ... & Darwish, M. A. (2022). Structure, morphology and electrical/magnetic properties of Ni-Mg nano-ferrites from a new perspective. Nanomaterials, **12**(7), 1045.

Vishwarup, R., & Mathad, S. N. (2020). Elastic properties of nano Mg1-xCoxFe2O4 (x= 0.15, 0.2, 0.25, 0.3, 0.35 and 0.4) synthesized by co-precipitation method. *Materials Science for Energy Technologies*, **3**, 559-565.

Mirbagheri, M., Mirzaee, O., Tajally, M., & Shokrollahi, H. **(2023).** Synthesis, structure, hyperthermia behavior and magnetic properties of Mn–Zn particles prepared by a new method of ball-milling and heating. *Physics Open*, 100139.

Thummer, K. P., Chhantbar, M. C., Modi, K. B., Baldha, G. J., & Joshi, H. H. (2004). 57Fe Mössbauer studies on MgAlxCrxFe2-2xO4 spinel system. *Materials Letters*, **58**(17-18), 2248-2251.

Thakur, A., Mathur, P., & Singh, M. (2007). Study of dielectric behaviour of Mn–Zn nano ferrites. *Journal of Physics and Chemistry of solids*, **68**(3), 378-381.

Thakur, P., Chahar, D., Taneja, S., Bhalla, N., & Thakur, A. (2020). A review on MnZn ferrites: Synthesis, characterization and applications. *Ceramics international*, **46**(10), 15740-15763.

Chhaya, U. V., & Kulkarni, R. G. (1999). Metal-insulator type transition in aluminium and chromium co-substituted nickel ferrites. *Materials Letters*, **39**(2), 91-96.

Thummer, K. P., Tanna, A. R., & Joshi, H. H. (2017, May). Rietveld structure refinement and elastic properties of MgAlxCrxFe2− 2xO4 spinel ferrites. In *AIP Conference Proceedings*, **1837**(1), **040058**. AIP Publishing LLC.

Bhatu, S. S., Lakhani, V. K., Tanna, A. R., Vasoya, N. H., Buch, J. U., Sharma, P. U., ... & Modi, K. B. (2007). Effect of nickel substitution on structural, infrared and elastic properties of lithium ferrite.

O'horo, M. P., Frisillo, A. L., & White, W. B. (1973). Lattice vibrations of MgAl2O4 spinel. *Journal of Physics and Chemistry of Solids*, **34**(1), 23-28.

Modi, K. B., Rangolia, M. K., Chhantbar, M. C., & Joshi, H. H. (2006). Study of infrared spectroscopy and elastic properties of fine and coarse grained nickel–cadmium ferrites. *Journal of materials science*, **41**, 7308-7318.

Waldron, R. D. (1955). Infrared spectra of ferrites. *Physical review*, **99**(6), 1727.

Kakani, S. L., and Hemrajani, C., Statistical Mechanics. India, Viva Books Private Limited, 2017.